

Two component spin-fermion model for high- T_c cuprates: Applications to neutron scattering and ARPES experiments

Yunhyu Bang

Department of Physics, Chonnam National University, Kwangju 500-757, Korea

Motivated by neutron scattering experiments in the high- T_c cuprates, we propose the two-component spin-fermion model as a minimal phenomenological model which has both local spins and itinerant fermions as independent degrees of freedom. Our calculations of the dynamic spin correlation function provide a successful description of the puzzling neutron experiment data and show that: (1) the upward dispersion branch of magnetic excitations is mostly due to the local spin excitations; (2) the downward dispersion branch is from collective particle-hole excitations of fermions; and (3) the resonance mode is a mixture of both degrees of freedom. Using the same model with the same set of parameters we calculated the renormalized quasiparticle dispersion and successfully reproduced one of the key features of the angle resolved photoemission spectroscopy (ARPES) experiments, i.e., the high energy kink structure in the fermion quasiparticle dispersion, hence further support the two component spin-fermion phenomenology.

PACS numbers: 74.72.-h, 75.30.Ds, 78.70.Nx, 74.25.Jb

I. INTRODUCTION

The study of spin dynamics has been a key research interest since the discovery of the high- T_c superconductor because it is expected that the spin correlation holds crucial information for the mechanism of the high- T_c superconductivity (HTS). For long the two main observations in the neutron scattering experiments of high- T_c cuprates (HTC) are (1) the incommensurate (IC) peaks at low energy or at quasielastic excitations^{1,2} and (2) the so-called resonance peak at commensurate wave vector at relatively high energy ($30 \sim 50$ meV)³⁻⁵. In early experiments the IC peaks were observed only in the deeply underdoped lanthanum cuprate and the resonance mode was the hallmark of the fully doped two layer yttrium cuprate. However, later experiments reveal that both features appear in both groups of cuprate compounds, although sensitively depending on doping level. More recently with inelastic neutron scattering (INS) experiments⁶⁻¹¹ with high precision, an unifying form of the magnetic excitations in the cuprate superconductors has emerged as "hourglass" shape of excitations around the wave vector $(1/2, 1/2)$ (hereafter in units of $2\pi/a$), in which the low energy IC excitations form the downward dispersion branch and the high energy IC excitations form the upward dispersion branch, and the two branches of excitations merge at the commensurate momentum $\mathbf{Q}=(1/2, 1/2)$ and at the resonance frequency Ω_{res} .

It is a pressing question to understand the origin of this "hourglass" shape excitations. Theoretical proposals up to now can be classified into two groups: (1) theories based on the spin dynamics in the presence of stripes¹²⁻¹⁵, and (2) Fermi liquid type theories of itinerant fermions¹⁶⁻²⁰. The key idea of the first group of theories is that the stripes formed by doping in the two dimensional Cu-O plane splits the commensurate spin wave excitations into two IC branches at the wave vectors $(1/2 \pm \delta, 1/2)$ or at their symmetry rotated positions by $x \longleftrightarrow y$ depending on the directions of the stripes. The dispersions from each branch of the two IC modulation cross at the commensurate wave vector $(1/2, 1/2)$ at a higher energy, which is then identified as the resonance mode. This picture provides a qualitative explanation to the hourglass dispersion and the resonance mode. However, this type of theories has difficulty to be extended to the higher doping regime where the presence and the nature of the stripes is questionable. The second group of proposals are itinerant fermion theories with interaction¹⁶⁻²⁰. In this type of theories, the resonance mode and the downward dispersion can be obtained, but the upward dispersion branch is not yet satisfactorily reproduced.

In this paper, we propose a two component spin-fermion model^{21,22} as a minimal phenomenological model to provide a natural and unifying explanation of the above mentioned neutron experiments of HTC. In this phenomenological model, the minimal set of low energy degrees of freedom are the spin wave excitations of local spins and the continuum particle-hole excitations of fermions. A similar phenomenological theory is also known as one component spin-fermion model and has been intensively studied by Pines and coworkers²³. The main difference of the two component model from the one component one is the introduction of the spin wave excitations directly from the local spins in addition to the usual collective spin density excitations from fermions. In this paper, we show that the presence of the local spin fluctuations is essentially proven by the INS and angle resolved photoemission spectroscopy (ARPES) experiments of HTC, therefore supporting the two component spin-fermion model as a minimal phenomenological model of HTS.

II. FORMALISM

In a mixed momentum and real-space representation the two component spin-fermion phenomenology Hamiltonian is written as

$$H = \sum_{\mathbf{k}, \alpha} c_{\alpha}^{\dagger}(\mathbf{k}) \varepsilon(\mathbf{k}) c_{\alpha}(\mathbf{k}) + \sum_{\mathbf{r}, \alpha, \beta} g \vec{\mathbf{S}}(\mathbf{r}) \cdot c_{\alpha}^{\dagger}(\mathbf{r}) \vec{\sigma}_{\alpha\beta} c_{\beta}(\mathbf{r}) + H_S(\vec{\mathbf{S}}(\mathbf{r})), \quad (1)$$

where the first term is the fermionic kinetic energy and the second term describes the coupling between local spins $\vec{\mathbf{S}}(\mathbf{r})$ and the spin density of the conduction electrons $\vec{\mathbf{s}}(\mathbf{r}) = c_{\alpha}^{\dagger}(\mathbf{r}) \vec{\sigma}_{\alpha\beta} c_{\beta}(\mathbf{r})$. The last term $H_S(\vec{\mathbf{S}}(\mathbf{r}))$ represents an effective low-energy Hamiltonian for the local spins $\vec{\mathbf{S}}(\mathbf{r})$. Instead of specifying H_S and solving it, we assumed a phenomenological Ansatz of the bare (before coupling to the fermions) local spin dynamics $\langle \vec{\mathbf{S}}_q \vec{\mathbf{S}}_{-q} \rangle_{\Omega} = \chi_{0,S}(\mathbf{q}, \Omega)$ with a short range AFM correlation, which has the general form as follows²⁴.

$$\chi_{0,S}^{-1}(\mathbf{q}, \Omega) = \chi_{0,S}^{-1}(\mathbf{Q}, 0) \cdot [1 + \xi^2 |\mathbf{q} - \mathbf{Q}|^2 - \Omega^2 / \Delta_{SG}^2], \quad (2)$$

where \mathbf{Q} the 2D AFM ordering vector, and the spin gap energy Δ_{SG} and the magnetic correlation length ξ combine to give the spin wave velocity $v_s = \Delta_{SG} \cdot \xi$ which can be determined by direct measurement²⁵.

The key difference of the Hamiltonian Eq.(1) from the one component Hamiltonian²³ is the definition and meaning of the spin fields $\vec{\mathbf{S}}(\mathbf{r})$. We assumed that $\vec{\mathbf{S}}(\mathbf{r})$ is the local spin degrees of freedom (d.o.f.) besides and independent from fermions $c_{\alpha}^{\dagger}(\mathbf{r})$ and related itinerant spin density $\vec{\mathbf{s}}(\mathbf{r}) = c_{\alpha}^{\dagger}(\mathbf{r}) \vec{\sigma}_{\alpha\beta} c_{\beta}(\mathbf{r})$. On the other hand, in one component spin-fermion model²³, the collective spin fields is defined as the itinerant spin density operator made of fermions, hence fundamentally linked to the fermions, and there is no concept of the local spins. Another important distinct feature of our two component phenomenology is the local spin dynamics defined in Eq. (2). This form of the local spin correlation function with a short range AFM order should be valid not only near \mathbf{Q} but also for the entire BZ of \mathbf{q} – if the precise form of the spin-wave dispersion is ignored – because at high energies the local spin dynamics becomes less sensitive to the long range order or short range order. However, the similar form of the itinerant spin correlation function assumed in the one component model²³ is valid only in a narrow region of \mathbf{q} around \mathbf{Q} by definition.

Microscopic justification of the above two component model, starting, for example, from Hubbard or t-J model, is the heart of problem of HTC for the last twenty years or so. We can only sketch here the underlying idea for our phenomenology. Starting from a Hubbard model, for example, dynamic mean field theory (DMFT)²⁶ demonstrated that the key consequence of the strong correlation of large U Coulomb interaction is to split the electron spectral density into two parts: one near the Fermi level - the itinerant one, and the other at the lower and upper Hubbard bands far below and above the Fermi level - hence the localized one. Therefore this splitting of one bare electron spectral density into the itinerant and localized parts is not a new observation but has already had a solid theoretical justification.

A new step in our phenomenology is to propose that the localized spectral density far away from the Fermi level is not dormant for the low energy physics. In the framework of the DMFT, once the coherent band is formed at the Fermi level in addition to the upper and lower Hubbard bands through the strong correlation effect, the low energy physics is solely described by the coherent band near Fermi level and the Hubbard bands appear only as high energy charge fluctuations such as the incoherent absorption bands at high frequencies of order $O(U)$, for example, in optical conductivity. This picture is correct with respect to the charge degree of freedom because the DMFT is designed to capture the strong correlation of charge dynamics by being a single site impurity model. However, it is physically rather obvious that the localized Hubbard bands can still contribute to low energy physics through spin fluctuations. In order to capture this low energy spin degree of freedom, it is, however, necessary to study the lattice model – not a small cluster but thermodynamically large lattice. Then we have to give up all the merits of the DMFT. At the moment, there is no satisfactory microscopic theory for the lattice model which faithfully treats the strong correlation of large U .

To this end, we note that there exist two spin correlation functions in our two component model: χ_S the one from the local spins $\vec{\mathbf{S}}(\mathbf{r})$ and χ_f the one from the itinerant spin density $\vec{\mathbf{s}}(\mathbf{r}) = c_{\alpha}^{\dagger}(\mathbf{r}) \vec{\sigma}_{\alpha\beta} c_{\beta}(\mathbf{r})$. Counting the coupling term to one loop order (equivalent to the RPA), the dressed spin correlation functions of the Hamiltonian (1) are written as follows.

$$\chi_S^{-1}(\mathbf{q}, \Omega) = \chi_{0,S}^{-1}(\mathbf{q}, \Omega) - g^2 \cdot \chi_{0,f}(\mathbf{q}, \Omega) \quad (3)$$

$$\chi_f^{-1}(\mathbf{q}, \Omega) = \chi_{0,f}^{-1}(\mathbf{q}, \Omega) - g^2 \cdot \chi_{0,S}(\mathbf{q}, \Omega) \quad (4)$$

where $\chi_{0,S}$ is introduced in Eq. (2) and $\chi_{0,f}$ is the noninteracting spin susceptibility of the conduction band of the fermions. The diagrammatic illustration of the derivation of Eqs.(3) and (4) is shown in Fig.1. The noninteracting spin susceptibility $\chi_{0,f}$ is written as

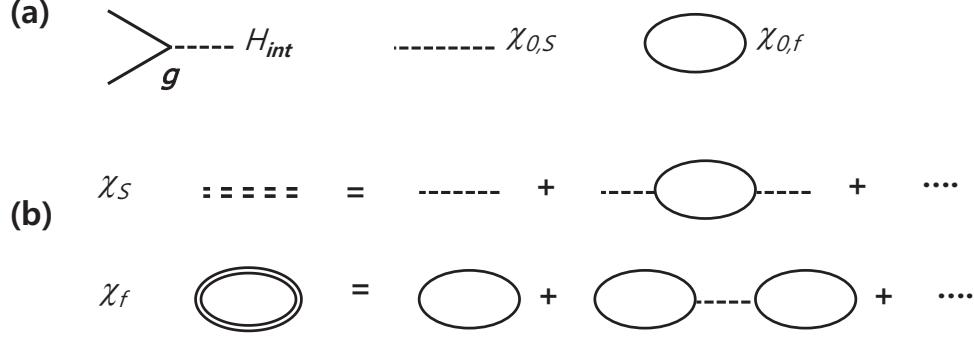


FIG. 1: (a) Interaction vertex of H_{int} , and bare spin correlation functions $\chi_{0,S}$ and $\chi_{0,f}$. (b) The graphic illustration of summations of the infinite series for the dressed spin correlation functions χ_S and χ_f as defined in Eqs.(3) and (4)

$$\begin{aligned}
\chi_{0,f}(\mathbf{q}, \Omega) &= \sum_k \frac{1}{2} \left[1 + \frac{\boldsymbol{\varepsilon}(\mathbf{k} + \mathbf{q})\boldsymbol{\varepsilon}(\mathbf{k}) + \Delta(\mathbf{k} + \mathbf{q})\Delta(\mathbf{k})}{E(\mathbf{k} + \mathbf{q})E(\mathbf{k})} \right] \\
&\times \frac{f(E(\mathbf{k} + \mathbf{q})) - f(E(\mathbf{k}))}{\omega - [E(\mathbf{k} + \mathbf{q}) - E(\mathbf{k})] + i\Gamma} \\
&+ \sum_k \frac{1}{4} \left[1 - \frac{\boldsymbol{\varepsilon}(\mathbf{k} + \mathbf{q})\boldsymbol{\varepsilon}(\mathbf{k}) + \Delta(\mathbf{k} + \mathbf{q})\Delta(\mathbf{k})}{E(\mathbf{k} + \mathbf{q})E(\mathbf{k})} \right] \\
&\times \frac{1 - f(E(\mathbf{k} + \mathbf{q})) - f(E(\mathbf{k}))}{\omega - [E(\mathbf{k} + \mathbf{q}) + E(\mathbf{k})] + i\Gamma} \\
&+ \sum_k \frac{1}{4} \left[1 - \frac{\boldsymbol{\varepsilon}(\mathbf{k} + \mathbf{q})\boldsymbol{\varepsilon}(\mathbf{k}) + \Delta(\mathbf{k} + \mathbf{q})\Delta(\mathbf{k})}{E(\mathbf{k} + \mathbf{q})E(\mathbf{k})} \right] \\
&\times \frac{f(E(\mathbf{k} + \mathbf{q})) + f(E(\mathbf{k})) - 1}{\omega + [E(\mathbf{k} + \mathbf{q}) + E(\mathbf{k})] + i\Gamma}, \tag{5}
\end{aligned}$$

where $E(\mathbf{k}) = \sqrt{\boldsymbol{\varepsilon}^2(\mathbf{k}) + \Delta^2(\mathbf{k})}$ and the itinerant fermion dispersion $\boldsymbol{\varepsilon}(\mathbf{k})$ is given by a tight binding model

$$\boldsymbol{\varepsilon}(\mathbf{k}) = -2t(\cos(k_x) + \cos(k_y)) - 2t' \cos(k_x) \cdot \cos(k_y) - \mu. \tag{6}$$

For calculations in this paper, we chose $t' = -0.4t$, and $\mu = -0.81t$. The overall energy scale t and the choice of parameters t' , μ will be discussed later with the numerical results. For the superconducting state (SS), we assume a canonical d-wave gap function $\Delta(\mathbf{k}) = \Delta_0[\cos(k_x) - \cos(k_y)]$ and for the normal state (NS), we set $\Delta_0 = 0$ in Eq.(5).

Having two degrees of freedom in the model, two spin susceptibilities χ_S and χ_f should be calculated on equal footing. Previous studies of the local spin correlation embedded in the fermion bath²⁴ considered only the imaginary part of $\chi_{0,f}$ (so called Landau damping) in Eq. (3) to damp the spin wave excitations of Eq. (2) and the real part of $\chi_{0,f}$ is assumed either already included in the definition of the bare local spin dynamics described in Eq. (2) or having negligible effects. In fact, when the coupling g is weak, this approach is reasonable. But in the strong coupling limit when the dimensionless coupling constant $\lambda \equiv g^2 \cdot \chi_{0,f}(\mathbf{Q}, 0) \cdot \chi_{0,S}(\mathbf{Q}, 0) \sim O(1)$, it is crucial to include both the real and imaginary parts as in the above equations (3) and (4). As we can see in the next section, in the strong coupling limit both dressed spin susceptibilities $\chi_S(\mathbf{q}, \Omega)$ and $\chi_f(\mathbf{q}, \Omega)$ become a mixture of the local spins and the itinerant fermions and they assimilate to each other with increasing the coupling strength λ .

In passing, the Eqs. (3) and (4) are loop expansions (one loop order) but not a coupling constant expansion. Therefore, the strong coupling limit of $\lambda \sim O(1)$ is not a problem, but the higher loop diagrams – for example, vertex corrections in a standard many body terminology – need to be worried. This question is the beyond the scope of the current work.

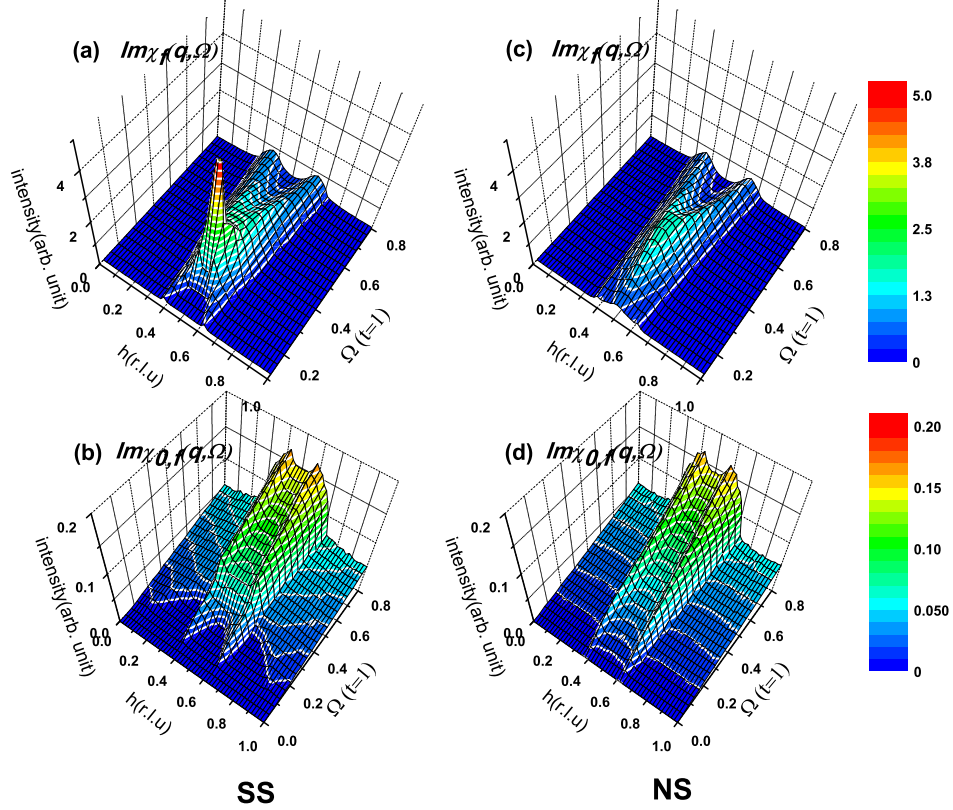


FIG. 2: (Color online) (a-b, in the left column) The dressed itinerant spin susceptibility $Im\chi_f(\mathbf{q} = (h, 1/2), \Omega)$ and the bare spin susceptibility $Im\chi_{0,f}(\mathbf{q}, \Omega)$, respectively, in the superconducting state. Parameters are $\Delta_{SG} = 1.1t$, $\Delta_0 = 0.2t$, and $\lambda = 0.8$; (c-d, in the right column) $Im\chi_f(\mathbf{q}, \Omega)$ and $Im\chi_{0,f}(\mathbf{q}, \Omega)$, respectively, in the normal state ($\Delta_0 = 0$).

III. NEUTRON SCATTERING

In order to study the INS experiments, we calculated the fully dressed dynamic spin susceptibilities $\chi_S(\mathbf{q}, \Omega)$ and $\chi_f(\mathbf{q}, \Omega)$ of Eqs. (3) and (4). As mentioned in the previous section, in the strong coupling limit of $\lambda \sim O(1)$, the behaviors of $\chi_S(\mathbf{q}, \Omega)$ and $\chi_f(\mathbf{q}, \Omega)$ become qualitatively similar each other. Therefore, we conveniently discuss the numerical results of $\chi_f(\mathbf{q}, \Omega)$ in this paper. But for completeness, we also show the numerical results of $\chi_S(\mathbf{q}, \Omega)$ as well as the total spin susceptibility $\chi_{tot} = \chi_f + \chi_S$, too.

A. $\chi_f(\mathbf{q}, \Omega)$ along $(0, 1/2) \rightarrow (1, 1/2)$

Figure 2(a) shows $Im\chi_f(\mathbf{q}, \Omega)$ scanned along $\mathbf{q} = (h, 1/2)$ in the SS. The superconducting gap $\Delta_0 = 0.2t$, the bare spin gap $\Delta_{SG} = 1.1t$ (it is not the physical spin gap), and the dimensionless coupling constant $\lambda = 0.8$ ($g^2 = 0.95 \text{ eV}^2$) were chosen. The main effect of the coupling is to renormalize down the bare spin gap energy Δ_{SG} below the particle-hole excitation gap of $\chi_{0,f}(\mathbf{q}, \Omega)$ ($\sim 2\Delta_0$), which then forms a sharp resonance peak at $\mathbf{Q} = (1/2, 1/2)$. Centering from this resonance mode, both the downward dispersion branch and the upward dispersion branch span out. The origin of the upward dispersion is apparently from the local spin wave mode (see Eq. (2)) and the origin of the downward dispersion is the itinerant spin excitations of $\chi_{0,f}$. The latter fact can be identified in Fig. 2(b) which shows the non-interacting fermion spin susceptibility $Im\chi_{0,f}(\mathbf{q}, \Omega)$ scanned along $\mathbf{q} = (h, 1/2)$ in the SS. The shape and strength of the downward whisker like excitations in $Im\chi_{0,f}$ is sensitive to the Fermi surface (FS) curvature (controlled by μ and t'), and the size of the d-wave gap $\Delta(\mathbf{k}) = \Delta_0[\cos(k_x) - \cos(k_y)]$.

With the coupling strength $\lambda = 0.8$, the dressed fermion spin susceptibility $\chi_f(\mathbf{q}, \Omega)$ obtains features of both the local spin susceptibility $\chi_{0,S}$ and the itinerant spin susceptibility $\chi_{0,f}$. In particular, the high energy parallel branches in $\chi_{0,f}$ (see Fig. 2(b) and (d)) are overwhelmed by the spin wave like excitations of $\chi_{0,S}$ in the dressed susceptibility χ_f as seen in Fig. 2(a) and (c). With a smaller coupling strength ($\lambda < 0.5$) the two spin susceptibilities $\chi_S(\mathbf{q}, \Omega)$ and $\chi_f(\mathbf{q}, \Omega)$ retain more of their bare characteristics of the spin wave excitations and the itinerant fermion susceptibility, respectively, and the resonance peak at

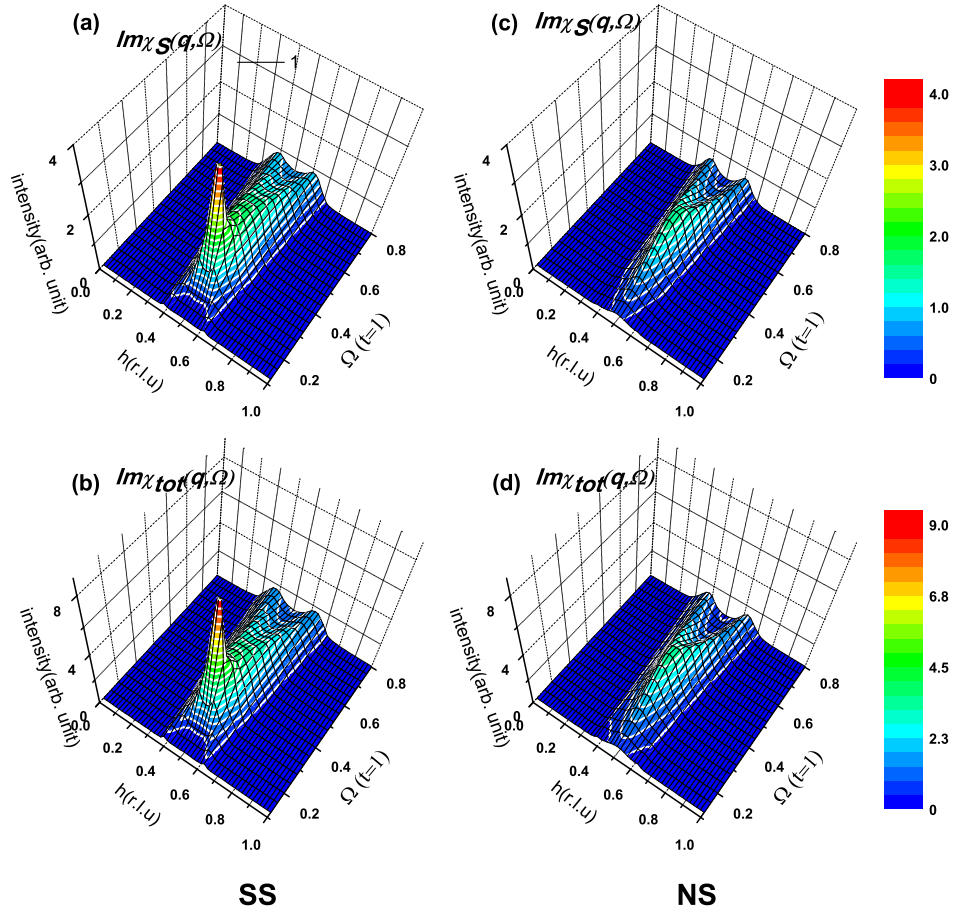


FIG. 3: (Color online) (a-b, in the left column) The dressed local spin susceptibilities $Im\chi_S(\mathbf{q}, \Omega)$ and the total spin susceptibilities $Im\chi_{tot}(\mathbf{q}, \Omega) = Im\chi_S + Im\chi_f$, respectively, in the superconducting state. (c-d, in the right column) $Im\chi_S(\mathbf{q}, \Omega)$ and $Im\chi_{tot}(\mathbf{q}, \Omega)$, respectively, in the normal state. Parameters are the same as in Fig.2.

$\mathbf{Q} = (1/2, 1/2)$ is not formed.

Figure 2(c,d) are the same plots as in Fig. 2(a,b) but in the NS. First, the resonance peak becomes severely overdamped having only a hump like structure in $Im\chi_f(\mathbf{q}, \Omega)$. Second, the low energy downward whisker like dispersion disappears because the free fermion susceptibility $\chi_{0,f}(\mathbf{q}, \Omega)$ in the NS (see Fig. 2(d)) has no such structure. Lastly, the high energy upward dispersion remains almost similar to the case of the SS. The results of Fig. 2(a,c) successfully reproduce the main features of recent neutron scattering experiments in HTC^{6-11} , i.e., the resonance mode in SS, the hourglass shape of the upward and downward dispersions, and their drastic change between superconducting and normal states. In particular, these results strikingly resemble the INS data of $YBCO_{6.6}^{11}$. However, we need a reservation for applying our result to $L_{1.875}B_{x=0.125}CO_4^8$, which has a static stripe order and extremely low $T_c = 2.5$ K²⁷. In particular, the presence of the stripe ordering is likely to change the spin dynamics significantly¹³⁻¹⁵ and introduce the a-b plane anisotropy.

For comparison, we also show the numerical results of the local spin susceptibility $\chi_S(\mathbf{q}, \Omega)$ as well as the total spin susceptibility $\chi_{tot}(\mathbf{q}, \Omega) = \chi_f(\mathbf{q}, \Omega) + \chi_S(\mathbf{q}, \Omega)$ in Fig. 3. As mentioned above, the overall behavior of $\chi_S(\mathbf{q}, \Omega)$ is indistinguishably similar to $\chi_f(\mathbf{q}, \Omega)$ and so is $\chi_{tot}(\mathbf{q}, \Omega)$. This is the typical feature of the strong coupling limit of $\lambda \sim O(1)$ and remember that the value of $\lambda = 0.8$ used in our calculations was not an arbitrary choice but was determined by the (π, π) resonance condition. As expected, however, a fine difference exists so that, in general, $\chi_S(\mathbf{q}, \Omega)$, in comparison to $\chi_f(\mathbf{q}, \Omega)$, has a slightly more feature of the local spin dynamics at higher frequencies and a slightly less feature of the itinerant fermion spin dynamics at low frequencies and vice versa. For example, we can see a bit weaker downward dispersion branch in $\chi_S(\mathbf{q}, \Omega)$ in the SS (Fig.3(a)) than in $\chi_f(\mathbf{q}, \Omega)$ in the SS (Fig.2(a)).

Also although we plotted the total spin susceptibility as $\chi_{total} = \chi_f + \chi_S$, there is an ambiguity about whether the contributions from the local spin fluctuations χ_S and the itinerant spin fluctuations χ_f to the INS measurement should be equal as we tentatively

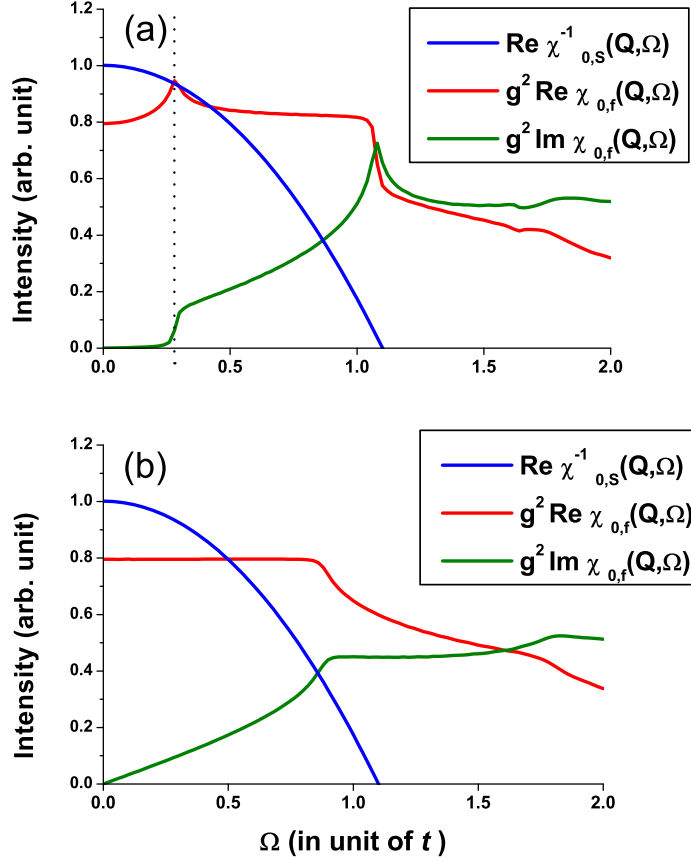


FIG. 4: (Color online) (a) Plots of bare susceptibilities $\text{Re}\chi_{0,S}^{-1}(\mathbf{Q}, \Omega)$, $g^2 \text{Re}\chi_{0,f}(\mathbf{Q}, \Omega)$, and $g^2 \text{Im}\chi_{0,f}(\mathbf{Q}, \Omega)$, respectively in superconducting state. Parameters are $\Delta_{SG} = 1.1t$, $\Delta_0 = 0.2t$, and $\lambda = 0.8$. The vertical dashed line is a guide to the eyes indicating the position of pole at $\Omega = 0.28t$. (b) The same as (a) in normal state (ie. $\Delta_0 = 0$).

assumed here because the form factors of the local and itinerant spins, in principle, should be different. However, our ignorance of the relative strength of the χ_f and χ_S fluctuations does not affect our phenomenology because the physical coupling strength between two spin fluctuations is determined by the effective dimensionless coupling $\lambda(q) \equiv g^2 \cdot \chi_{0,f}(\mathbf{q}, 0) \cdot \chi_{0,S}(\mathbf{q}, 0)$ and the value of $\lambda(\mathbf{Q})$ is determined once and for all by the (π, π) resonance condition and all other physical quantities are calculated without further ambiguity. Keeping this point in mind, the comparison of our numerical calculations to the INS experiments should be qualitatively the same whether we use the results of χ_f or χ_S , or χ_{tot} .

B. Origin of the resonance mode

The mechanism of forming the resonance mode in our model is illustrated in Fig. 4. When the inverse of the dressed susceptibilities of Eq. (3) and Eq. (4) crosses zero (which occurs simultaneously in both susceptibilities), the dressed susceptibilities develop a resonance mode: a bound state or an overdamped mode depending on the presence and strength of the imaginary part at the position of pole. In Fig. 4 we plot separately $\text{Re}\chi_{0,S}^{-1}(\mathbf{Q}, \Omega)$, $\text{Re}\chi_{0,f}(\mathbf{Q}, \Omega)$, and $\text{Im}\chi_{0,f}(\mathbf{Q}, \Omega)$ to make this point clear. Figure 4(a) is the case of a SS, where the pole of $\chi_{f,S}(\mathbf{q} = \mathbf{Q}, \Omega)$ occurs at $\Omega_{res} \sim 0.28t$. At this frequency the damping from $\text{Im}\chi_{0,f}$ is very weak below the p-h excitation gap, so that the pole becomes a sharp resonance peak. Figure 4(b) shows the case of the NS ($\Delta_0 = 0$) with the same parameters as in Fig. 2(c). The position of pole occurs at a little higher frequency ($\Omega \sim 0.5t$) compared to the case of the SC phase (Fig. 4(a)). But this pole is strongly damped by $\text{Im}\chi_{0,f}$ (green line) that is linearly increasing with energy, and this linearly increasing damping shifts down the actual position of the peak to $\Omega_{res} \sim 0.35t$ (the maximum height position in Fig. 2(c)). We note that this overdamped resonance peak at NS is consistent with the data of Ref¹¹ as shown in

Fig. 2(c).

The resonance mode found in our model has physically different content than the resonance mode in the Fermi liquid type theories¹⁶⁻¹⁹. The line of $Re\chi_{0,S}^{-1}(\mathbf{Q},\Omega)$ in Fig. 4 is not a simple inverse of a static potential (for example, $\frac{1}{U(q)}$ in a RPA calculation of Hubbard model as in¹⁷⁻¹⁹) but it carries its own dynamics and spectral density. Therefore, the resonance mode formed by coupling of two dynamic susceptibilities $\chi_{0,f}$ and $\chi_{0,s}$ should carry the spectral densities from both the local spin wave and the fermion particle-hole continuum. In our coupled two component spin-fermion model, the upward excitation branch and the resonance mode appear from a pole of Eq. (3) and Eq. (4) for a given \mathbf{q} but the downward excitation branch is made of particle-hole excitations of fermions in the d-wave SS and does not constitute a pole in Eq. (3) and Eq. (4). This is in contrast with the Fermi liquid type theories¹⁶⁻²⁰ where both the downward branch and the resonance mode are constructed by the pole of a RPA type spin susceptibility.

C. Constant energy scans

In the left column of Fig. 5.(a-d), we show the constant energy scans of $\chi_f(\mathbf{q},\Omega)$ in the SS for $\Omega = 0.2t, 0.28t, 0.6t$, and $0.8t$, respectively. Constant energy scans of neutron scattering data of YBCO⁷ and LBCO⁸ show peculiar patterns of IC peak positions in (q_x, q_y) momentum space at different energy cuts. In particular, the 45 deg rotation of the patterns from a low energy scan (below the resonance energy Ω_{res}) to a high energy scan drew special attention and several theoretical explanations have been proposed^{13-15,17-19}. Results of Fig. 5 demonstrate that the two component spin fermion model can consistently explain this phenomena, too.

Figure 5(b) in the left column is the scan of $\chi_f(\mathbf{q},\Omega)$ at the resonance energy, $\Omega_{res} = 0.28t$ with the same parameters as in Fig. 2(a). It shows a very intense peak at $(1/2, 1/2)$ indicating a very sharp resonance not only in energy but also in momentum space. Fig. 5(c) and Fig. 5(d) are the scans at higher energies than the resonance energy and Fig. 5(a) is a scan of lower energy cut. We colored the highest intensity positions with black color to emphasize the clear patterns. The lower energy scan (Fig. 5(a)) shows the IC peaks at $(1/2 \pm \delta, 1/2)$ and $(1/2, 1/2 \pm \delta)$ forming a diamond shape pattern. The higher energy scans (Fig. 5(c) and Fig. 5(d)) show that the IC peak positions at $(1/2 \pm \delta, 1/2 \pm \delta)$ and $(1/2 \pm \delta, 1/2 \mp \delta)$ forming a square shape pattern which has the symmetry of the 45 deg rotated from the low energy pattern. The results of Fig. 5 excellently reproduce the observed patterns of the constant energy scan data of neutron experiments reported in YBCO⁷ and LBCO⁸. This is rather surprising for LBCO since this compound is known to develop a static stripe ordering and our model has no ingredient for the stripes as we mentioned before.

In our model we can trace the origins of the IC peak patterns. The low energy IC peaks and diamond shape pattern is basically a reflection of the band structure and d-wave superconducting gap. The high energy IC peaks and the square shape pattern has more complicated origin. At and above the resonance energy the dressed spin susceptibility χ_f is the result of a strong interplay between the local spin correlation and the itinerant spin correlation. Therefore the high energy scan pattern is the result of a subtle interplay/competition between $\chi_{0,s}(\mathbf{q},\Omega)$ and $\chi_{0,f}(\mathbf{q},\Omega)$. The presence of IC peaks at high energies itself is the manifestation of the high energy spin wave dispersion spanning from the AFM wave vector \mathbf{Q} ; so the incommensurability increases with energy. However, whether the pattern will be a square or a diamond shape has no universal mechanism. We tested various combinations of parameters t' , μ , Δ_{SG} , Δ_0 and λ . The low energy diamond shape pattern is robust within our model. As to the patterns of higher energy scans, although the square shape is the dominant one, it is not absolutely robust; with different parameters the diamond pattern can appear, too. Therefore, we think that the 45 deg rotation of the IC peak patterns may not be an universal feature of HTC; it can change with doping and for different cuprate compounds. This non-universality is also seen in the scan of $\chi_S(\mathbf{q},\Omega)$ at $\Omega_{res} = 0.6t$ in the center column of Fig. 5(c). However, as repeatedly emphasized, the patterns of the constant energy scans for $\chi_S(\mathbf{q},\Omega)$, $\chi_{tot}(\mathbf{q},\Omega)$, and $\chi_f(\mathbf{q},\Omega)$ are basically the same each other in the strong coupling limit.

D. Parameters of our phenomenology

To make a comparison of our calculations with experiments, it is important to fix the energy scale of the model. The tight binding band of Eq. (6) is widely studied to fit the ARPES data and the estimate of t varies from 150 meV to 400 meV depending on the doping and different cuprate compounds²⁸. Our calculation results are in good agreement with neutron experiments in terms of energy scale if we choose $t \sim 150-180$ meV. This value of t corresponds to the low end of the estimates from ARPES experiments. One possible reason for it is that the extraction of t value from ARPES is carried by fitting the whole Brillouin zone (BZ) of the quasiparticle (q.p.) dispersions. As a result the high energy dispersion sets the overall energy scale t . However, the low energy spin susceptibility is determined by the low energy particle-hole excitations near Fermi level and irrelevant with the high energy q.p. excitations. With this reasoning it is quite possible that the effective t value near FS is in fact much reduced by a renormalization due to the strong correlation effect.

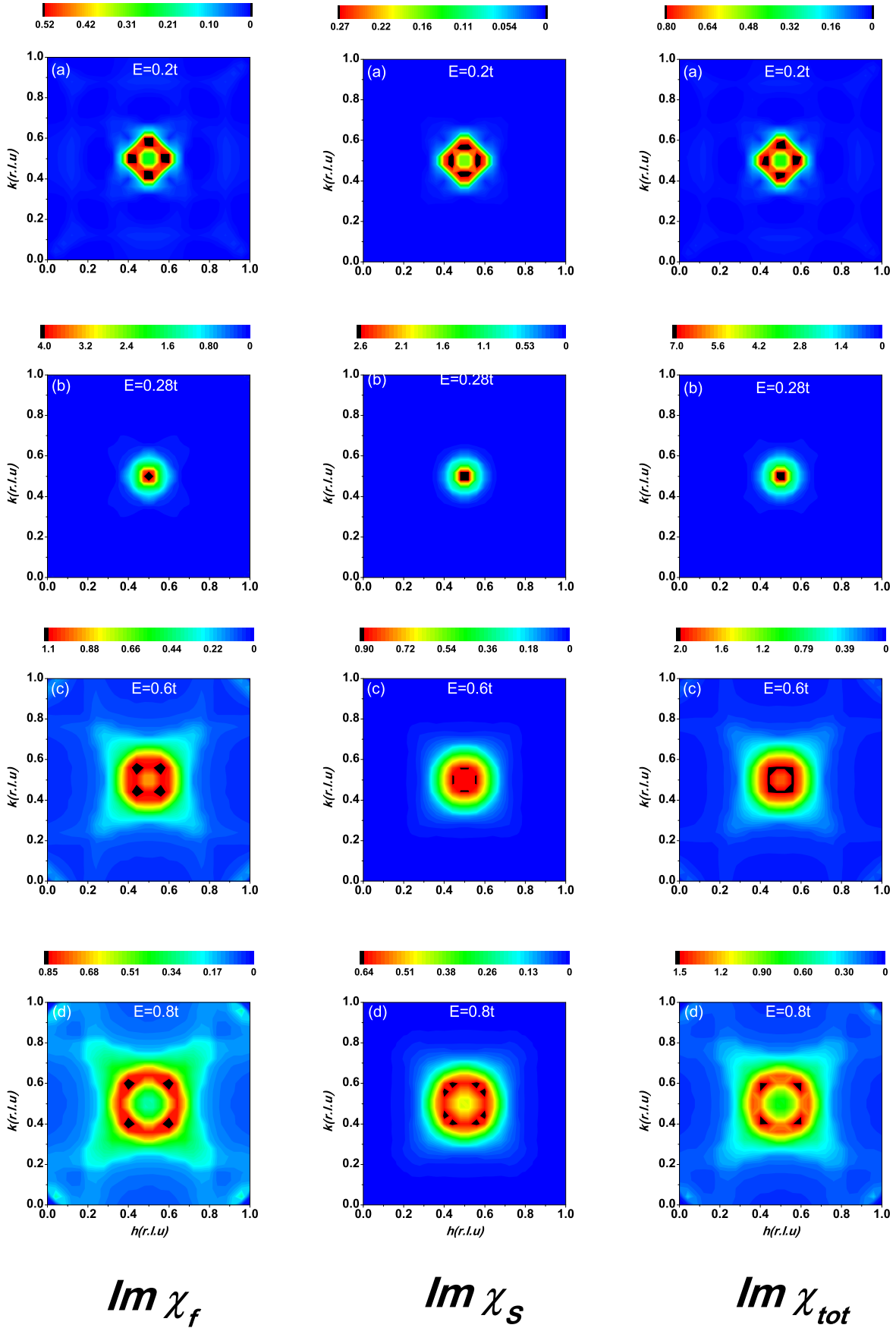


FIG. 5: (Color online) Constant energy scans of $Im \chi_f(\mathbf{q}, \Omega)$ (left column), $Im \chi_S(\mathbf{q}, \Omega)$ (center column), and $Im \chi_{tot}(\mathbf{q}, \Omega)$ (left column) at (a) $\Omega = 0.2t$, (b) $\Omega = 0.28t$, (c) $\Omega = 0.6t$, and (d) $\Omega = 0.8t$, respectively. In all cases, parameters are $\Delta_{SG} = 1.1t$, $\Delta_0 = 0.2t$, and $\lambda = 0.8$.

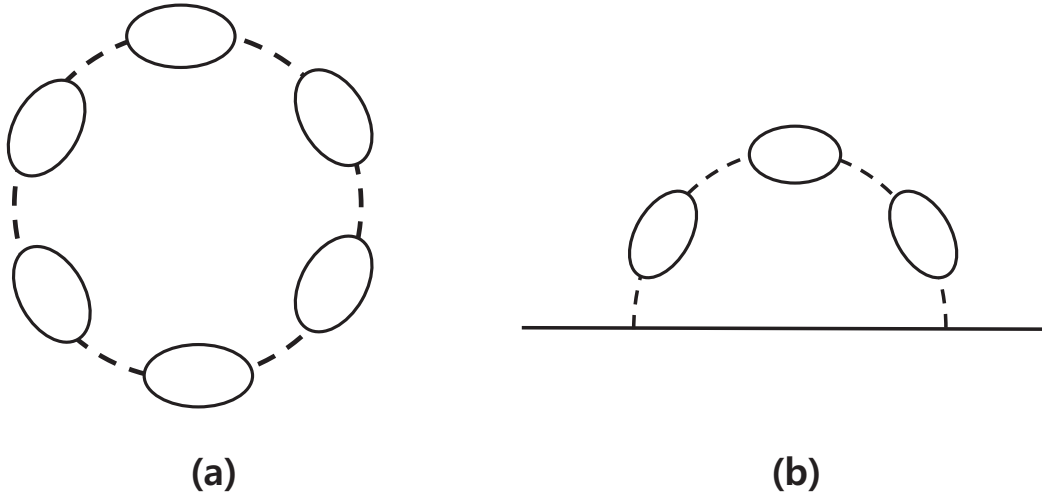


FIG. 6: (a) A typical diagram of the Free energy of the model Hamiltonian H of Eq.(1) in one loop approximation. (b) A typical diagram of the fermion selfenergy in one loop approximation calculated in Eq.(7). The diagram (b) can be obtained by cutting any fermion line of the diagram (a).

The degree of incommensurability and the strength of the downward whisker-like dispersion in the fermion susceptibility $\chi_{0,f}$ (see Fig. 2(b)) is controlled by the FS curvature – which is tuned by t' and the chemical potential μ – and the SC gap size Δ_0 ; this property is true even for the Fermi liquid theories or one component spin-fermion theories^{16–19}. These parameters t' , μ , and Δ_0 should be independently determined by other experiments such as ARPES²⁸, tunneling²⁹, etc. Therefore, after fixing the overall energy scale of the model by t , the genuinely free fitting parameters of our phenomenological model are only two: the coupling strength g (or equivalently λ) and the bare spin gap Δ_{SG} . For all calculations in this paper we used $t' = -0.4t$, $\mu = -0.81t$, $\Delta_0 = 0.2t$, $\Delta_{SG} = 1.1t$, and $\lambda=0.8$.

IV. ARPES AND HIGH ENERGY KINK

As a consistent check for our phenomenological model, we calculate the renormalized band dispersion with the same parameter set that we have used for the neutron scattering in previous section. In this calculation, the most important parameter is the coupling strength between fermions and spin fluctuations, for which there is no direct experimental measurement nor a reliable theoretical estimate from a microscopic Hamiltonian. In our phenomenology, this value $\lambda \equiv g^2 \cdot \chi_{0,f}(\mathbf{Q}, 0) \cdot \chi_{0,S}(\mathbf{Q}, 0) = 0.8$ was determined by the condition to produce (π, π) resonance mode both in the superconducting and normal states. So we can crosscheck the consistency of our phenomenology by comparing the outcomes of the q.p. renormalization from the spin-fermion interaction to the ARPES experiments.

The selfenergy of the fermion q.p. is calculated in Born approximation with the fully dressed local spin fluctuations $\chi_S(q, \omega)$ as

$$\Sigma(\vec{k}, \omega) = g^2 \sum_q \int \frac{d\omega'}{\pi} \frac{Im\chi_S(q, \omega')}{\omega + \omega' - \epsilon_{k+q} + i\Gamma} [n(\omega') + f(\epsilon_{k+q})] \quad (7)$$

where $n(\omega)$ and $f(\omega)$ are the Boson and Fermion distribution functions, respectively. Notice that this calculation of the fermion selfenergy is the same one loop approximation as the calculations of the spin susceptibility renormalization in Eqs.(3) and (4), guaranteeing the consistency of our phenomenology. This is graphically demonstrated in Fig. 6. We then calculate the renormalized q.p. spectral density as $A(\vec{k}, \omega) = ImG_R(\vec{k}, \omega)$ with $G_R(\vec{k}, \omega) = \frac{1}{\omega - \epsilon_k - \Sigma(\vec{k}, \omega)}$.

In Fig. 7, we show the contour plots showing the intensity of the q.p. spectral densities with and without the selfenergy correction. Fig. 7(a-b) show the dispersions along the nodal direction $(0, 0) \rightarrow (\pi, \pi)$ and Fig. 7(c-d) show the dispersions along the near antinodal direction $(0, 0.5\pi) \rightarrow (\pi, 0.5\pi)$. Two features are distinctively seen as results of the spin-fermion interaction: (1) the overall q.p. dispersion is renormalized by a factor of $\sim O(2)$. This is consistent with the input $\lambda = 0.8$ because the wave

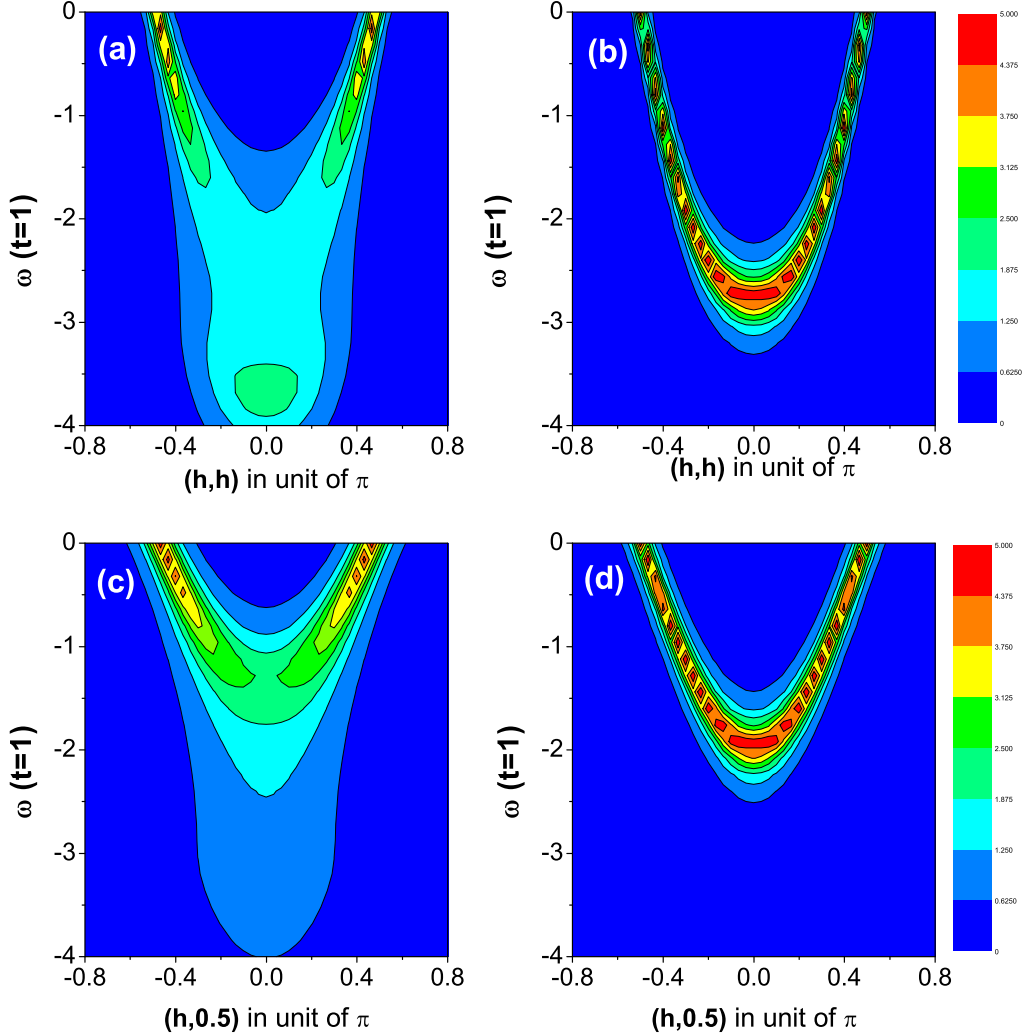


FIG. 7: (Color online) Spectral densities of quasiparticle dispersions: (a, c) Renormalized band dispersions along (h,h) and $(h, 0.5)$ cuts, respectively. (b, d) Bare band dispersions along (h,h) and $(h, 0.5)$ cuts, respectively.

function renormalization factor is $Z \approx (1 + \lambda)$; (2) much interesting point is that the q.p.s with a certain energy below the Fermi level are so strongly renormalized that the bare dispersion is not continuously renormalized but is detached from the low energy dispersion and forms a broad spectral puddle at further high energy region (see Fig. 7(a) and (c)).

This second feature is commonly observed both for the nodal and antinodal directions regardless of some differences of the fine details such as the breaking points of dispersion in energy and momentum space and the intensity of the broad spectral puddle at high energies. This behavior is remarkably similar to the so-called high energy kinks ($\sim 340meV$) observed in the ARPES experiments with BSCCO and LBCO by T. Valla *et al*²⁷ The breaking point of the dispersion occurs around $\omega \sim 1.5 - 2t$ in our model calculations. In fact, if we assume $t \sim 150 - 180meV$ as discussed before, the kink energy we calculated corresponds to $\sim 225 - 360meV$, consistent with the experimental data. Our results even reproduce the overall differences of the dispersion and kink behavior between the nodal direction and the antinodal direction as observed in experiments.²⁷

We can trace the origin of this jump or breaking of the q.p. dispersion and found that it is caused by the upper bound of the local spin wave excitations $\chi_S(\mathbf{q}, \Omega)$. The local spin wave excitations, defined in Eqs.(2) and (3), disperses from the lowest energy $\tilde{\Delta}_{SG}$ (renormalized one) at $\mathbf{q} = \mathbf{Q} = (\pi, \pi)$ to the highest energy at the magnetic zone corners $\mathbf{q} = (2\pi, 2\pi)$ and its equivalent points. Even after dressed by fermions as in Eq.(3) this damped spin wave excitations has a similar upper bound. With the parameters of our model, this high energy upper bound of the local spin fluctuations is limited at around $2t$. Physical meaning of it is that

the local spin excitations exist only up to $\sim 2t$ and the fermion q.p. cannot be scattered beyond this energy scale. Consequently the real part of selfenergy calculated with Eq.(7) develops a rapid variation at around $2t$ in frequencies and q.p. pole is not formed beyond this energy scale in the dressed fermion Green's function $G_R(\vec{k}, \omega) = \frac{1}{\omega - \varepsilon_k - \Sigma(\vec{k}, \omega)}$. Hence we can understand the origin of the high energy kink from the high energy upper bound of the local spin excitations³⁰. Consistency between our model calculations and experimental observation of the high energy kink strongly supports the existence and strength of local spin excitations which have a upper energy scale around 350meV . In contrast, the itinerant spin fluctuations has a long tail of the particle-hole continuum excitations up to the band width ($\sim 8t$) which would be a couple of eV at least. Therefore, the one component spin-fermion model with only the itinerant fermions would have a difficulty to explain the high energy kink phenomena.

The reproduction of the high energy kink feature in the renormalized q.p. dispersion also implies that not only the low energy spin excitations near (π, π) plays an important role but also the high energy spin excitations can play an important role. However, it doesn't necessarily mean that the coupling of the high energy spin excitations to fermions has a comparable strength as the coupling of the low energy spin excitations to fermions. In fact, the effective coupling between fermions and the local spins $\lambda(\mathbf{q})$ becomes much weaker with \mathbf{q} away from $\mathbf{Q} = (\pi, \pi)$. However, the phase space of the local spin excitations rapidly increases with increasing \mathbf{q} from $\mathbf{Q} = (\pi, \pi)$, which compensates for the weakness of coupling.

Within our resolution, we didn't find noticeable features in the low energy q.p. dispersion, i.e., the low energy kink, which might be related with the (π, π) resonance mode. Possibly it is because the spectral weight of the resonance mode in NS (see Fig. 3(c)) is not sufficiently dominant over the total spectral density of the spin fluctuations spread over the whole momentum space, and/or more possibly because the low energy kink is in fact not an abrupt kink but rather a gentle variation of the dispersion slope as seen in the recent experiment³¹.

V. CONCLUSION

In summary, we proposed a phenomenological two-component spin fermion model motivated by the neutron scattering experiments in HTC. With the two spin degrees of freedom of the local spins and the itinerant spins, our calculations of the dynamic spin susceptibilities coherently reproduced the essential features of the neutron experiments in HTC: the hourglass dispersions, resonance mode, their changes in normal and superconducting states, and the IC peak patterns of constant energy scans. Although our approach is a phenomenology, considering that there are genuinely only two free fitting parameters, i.e., the coupling constant λ and the bare spin gap Δ_{SG} , the successful reproduction of the several key features of neutron experiments with one set of parameters is quite encouraging. Then with the same model parameters, we calculated the renormalized fermion q.p. dispersion and reproduced both the nodal and antinodal high energy kinks with the correct energy scale in agreement with ARPES experiments²⁷. It further strengthened the justification for our phenomenology.

Finally, the main message of this work with the two component spin-fermion phenomenology is to demonstrate that there are compelling experimental evidences³² for the presence and its important role of the local spin degrees of freedom in addition to the fermionic quasiparticles in the cuprates. Interestingly, there are also accumulating experimental evidences for the coexistence of the itinerant electrons and local moment of spins in the recently found iron-based superconducting compounds^{33,34}. The pressing question is now what the microscopic theory is for the phenomenological two-component spin fermion model; in other words how the local spin degrees of freedom survives doping from the parent insulating cuprate compounds, or more generally how the local moments and the itinerant fermions coexist in the strongly correlated metallic systems such as cuprate and pnictide compounds.

The author (Y.B.) was supported by the Grant No. NRF-2010-0009523 and NRF-2011-0017079 funded by the National Research Foundation of Korea.

-
- ¹ Cheong S-W *et al* 1991 *Phys. Rev. Lett.* **67** 1791
² Dai P, Mook H A and Dogan F 1998 *Phys. Rev. Lett.* **80** 1738
³ Mook H A *et al* 1993 *Phys. Rev. Lett.* **70** 3490
⁴ Fong H *et al* 1995 *Phys. Rev. Lett.* **75** 316
⁵ Dai P, Mook H A, Aeppli G, Hayden S M and Dogan F 2000 *Nature* **406** 965
⁶ Arai M, Nishijima T, Endoh Y, Egami T, Tajima S, Tomimoto K, Shiohara Y, Takahashi M, Garrett A, and Bennington S M 1999 *Phys. Rev. Lett.* **83** 608
⁷ Hayden S M *et al* 2004 *Nature* **429** 531
⁸ Tranquada J M *et al* 2004 *Nature* **429** 534
⁹ Pailhes S, Sidis Y, Bourges P, Hinkov V, Ivanov A, Ulrich C, Regnault L P, and Keimer B 2004 *Phys. Rev. Lett.* **93** 167001
¹⁰ Hinkov V *et al* 2004 *Nature* **430** 650
¹¹ Hinkov V *et al* 2007 *Nature Physics* **3** 780

- 12 Batista C D, Ortiz G, and Balatsky A V 2001 *Phys. Rev. B* **64** 172508
- 13 Uhrig G S, Schmidt K P and Gruninger M 2004 *Phys. Rev. Lett.* **93** 267003
- 14 Seibold G and Lorenzana J 2006 *Phys. Rev. B* **73** 144515
- 15 Vojta M, Vojta T and Kaul R K 2006 *Phys. Rev. Lett.* **97** 097001
- 16 Dahm T, Manske D and Tewordt L 1998 *Phys. Rev. B* **58** 12454
- 17 Morr D K and Pines D 1998 *Phys. Rev. Lett.* **81** 1086
- 18 Norman M R 2007 *Phys. Rev. B* **75** 184514 ; Eremin I, Morr D K, Chubukov A. V and Bennemann K 2007 *Phys. Rev. B* **75** 184534
- 19 Eremin I, Morr D K, Chubukov A V, Bennemann K H and Norman M R, 2005 *Phys. Rev. Lett.* **94** 147001
- 20 Sega I and Prelovsek P, 2006 *Phys. Rev. B* **73** 092516
- 21 Bang Y, Martin I, and Balatsky A V 2002 *Phys. Rev. B* **66** 224501
- 22 Bang Y, Graf M J, Curro N J and Balatsky A V 2006 *Phys. Rev. B* **74** 054514
- 23 Chubukov A V, Pines D, Schmalian J 2003 in *The Physics of Superconductors* ed. Benneman K H and Ketterson J B (Berlin: Springer) and references therein.
- 24 Sachdev S, Chubukov A V, and Sokol A 1995 *Phys. Rev. B* **51** 14874
- 25 Coldea R, Hayden S M, Aeppli G, Perring T G, Frost C D, Mason T E, Cheong S-W and Fisk Z 2001 *Phys. Rev. Lett.* **86** 5377
- 26 Georges A, Kotliar G, Krauth W and Rozenberg M J 1996 *Rev. Mod. Phys.* **68** 13
- 27 Valla T, Kidd T E, Yin W-G, Gu G D, Johnson P D, Pan Z -H and Fedorov A V 2007 *Phys. Rev. Lett.* **98** 167003
- 28 Markiewicz R S, Sahrakorpi S, Lindroos M, Lin H, and Bansil A 2005 *Phys. Rev. B* **72** 054519; Norman M 1995 *Phys. Rev. B* **52** 615
- 29 Krasnov V M 2009 *Phys. Rev. B* **79** 214510
- 30 Macridin A, Jarrell M, Maier T, and Scalapino D J 2007 *Phys. Rev. Lett.* **99** 237001
- 31 Dahm T *et al* 2009 *Nature Physics* **5** 217
- 32 Tacon M. Le *et al* 2011 *Preprint* arXiv:1106.2641
- 33 Yang L X *et al* 2009 *Phys. Rev. Lett.* **102** 107002
- 34 Zhang Chenglin *et al* 2010 *Preprint* arXiv:1012.4065